A detailed test of mode-coupling theory on all time scales: Time domain studies of structural relaxation in a supercooled liquid

G. Hinze,[a] David D. Brace, S. D. Gottke, and M. D. Fayer
Department of Chemistry, Stanford University, Stanford, California 94305

(Received 14 March 2000; accepted 2 June 2000)

The dynamics of supercooled salol (phenyl salicylate) was measured in the time domain using optical Kerr effect techniques. By combining several experimental setups, data spanning more than six decades in amplitude and time ($\sim$100 fs to $\sim$1 μs) were observed. The data have a complex shape, ranging from high-frequency intramolecular oscillations at short times, to nearly exponential relaxation at long times. As predicted by mode-coupling theory (MCT), the data for some ranges of time appear as power laws. The slowest power law, the von Schweidler power law, has an almost constant exponent of $\sim$0.59 over the entire temperature range studied (247–340 K). Above the MCT T_c ($T > \sim 1.17\,T_g$, where T_g is the laboratory glass transition temperature) for $t > \sim 1$ ps, the decays are shown to be in excellent agreement with the master curve predicted by ideal MCT when higher order terms are included. However, the data do not display the plateau predicted by ideal MCT. To discuss the data at all temperatures, the intermediate time scale portion of the data, $2 < t < 10$ to 500 ps (depending on the temperature), is modeled as a power law that falls between the critical decay and the von Schweidler power law. This intermediate power law shows significant temperature dependence with an exponent that decreases to a value of ~ -1 below T_c. Calculations using extended MCT, for a full range of hopping times, demonstrate that the temperature dependence of the intermediate time scale data near and below T_c cannot be explained by extended MCT. © *2000 American Institute of Physics.* [S0021-9606(00)50833-2]

I. INTRODUCTION

The study of the liquids as they supercool and approach the glass transition involves effects that span a very broad range of times. The enormous slowing down of the complete structural relaxation with decreasing temperature is the most prominent feature of supercooled liquids. The slowing down is seen in macroscopic observables, like viscosity[1] and long time diffusion,[2] as well as in microscopic properties, like density fluctuations[3] and rotational correlation times.[4] Several phenomenological theories deal with the reduction in rates of processes in supercooled liquids.[5] However, dynamics in supercooled liquids cover such broad ranges of time and amplitude that a full understanding remains an experimental and theoretical challenge.

Mode coupling theory (MCT)[6,7] has been applied to the description of the dynamics in supercooled liquids. MCT treats the broad range of time scales, from ps to the longest decay times associated with complete structural relaxation. Because it provides detailed quantitative predictions of the relaxation behavior of supercooled liquids, MCT has triggered many recent experiments.[7–10] Interest in short times (ps-ns) or high frequencies (GHz-THz) has been stimulated by MCT. However, only a few experimental methods exist, e.g., dielectric spectroscopy[11,12] and dynamic light scattering,[13–17] which can cover a broad dynamic range. Most of the experimental methods used to study fast dynamics are frequency domain techniques, although there have been laser-based time domain measurements in the ps-ns region.[18,19] Some neutron scattering experiments permit acquisition of time domain data in the ps region.[20] While the accessible time window is very limited, the spatial resolution of neutron scattering can provide data that are very useful for comparison with the predictions of MCT.[20–22] In principle, time domain and frequency domain experiments can yield the same information. However, in practice, different aspects of the dynamics can be emphasized by various experiments.[23]

While supercooling and glass formation occur in a wide variety of materials, experimental investigations often focus on materials with simple structures. By selecting a molecule with relatively simple structure, contributions from intramolecular dynamics can be reduced or eliminated from the experimental observables. In this paper, we report a very detailed time domain experimental study of salol (phenyl salicylate) using the heterodyne detected optical Kerr effect (OKE) technique.[24–26] Salol forms a moderately fragile glass ($m \approx 60$)[27] with the melting temperature $T_m \cong 318$ K and the glass transition temperature $T_g \cong 220$ K. By combining several experimental setups, which are described in some detail below, we can measure the impulse response function of the polarizability–polarizability correlation function (orientational relaxation) from tens of fs to several μs and longer. The measurements can be made over any desired range of times with no gaps. In the experiments presented below, the data span more then six decades in time and six decades in amplitude. Salol has been the subject of a number of previous studies that have used a variety of experimental

[a]Permanent address: Institut fuer Physikalische Chemie, Johannes Gutenberg-Universität Mainz, Welderweg 15, 55099 Mainz, Germany.

methods.[28] The OKE technique can be seen as a complement to dynamic light scattering. However, as shown below, it is possible to extract new information on the dynamics from the time domain experiments. Preliminary results on salol have been published earlier.[26,29]

In the present paper, all of the features observed in the data on various time scales are addressed, from Raman active intramolecular vibrations at very short times to the α-relaxation (structural relaxation) at long times. The intermediate time scale data ($\sim$1 ps to $\sim$1 ns) is the most interesting. At the onset of the structural relaxation (the end of the intermediate time regime), the von Schweidler power law is observed. This power law has an almost constant exponent, $b \cong 0.59$, over the entire temperature range studied (247–340 K). At shorter times ($t < 2$ ps) somewhat above T_c, the data are compatible with the critical decay proposed by ideal MCT. Above the MCT T_c ($T > \sim 1.17\, T_g$, where T_g is the laboratory glass transition temperature) for $t > \sim 1$ ps, the decays are shown to be in truly remarkable agreement with the master curve predicted by ideal MCT when higher order terms are included. However, in contrast to the predictions of ideal MCT, complete structural relaxation occurs at all temperatures, even when $T < T_c$. The plateau predicted by ideal MCT is not observed. To examine the data over the full range of temperatures, the intermediate time scale portion of the data, $2 < t < 10$ to 500 ps (depending on the temperature), is modeled as a power law that falls between the critical decay and the von Schweidler power law. This intermediate power law shows significant temperature dependence with an exponent that decreases to a value of ~ -1 below T_c. Calculations using extended MCT, for a full range of hopping times, demonstrate that the temperature dependence of the intermediate time scale data, near and below T_c, cannot be explained by extended MCT.

II. EXPERIMENTAL PROCEDURES

The optical heterodyne detected optical Kerr effect experiment is a type of nonresonant pump–probe measurement.[24,25] The excitation pulse creates an optical anisotropy in the sample. Using short pulses $\leqslant$70 fs, the corresponding large bandwidth is sufficient to excite an orientationally anisotropic distribution of librations that add to the thermally excited isotropic librational distribution. Damping of the librations leaves behind a residual orientational anisotropy that decays by orientational relaxation.[30,31] If the pulse is longer, the bandwidth is too narrow to excite librations by stimulated Raman scattering. However, an anisotropy develops because the **E** field skews the thermal orientational fluctuations of molecules in the liquid. For either type of excitation, the decay of the induced anisotropy is monitored with an additional probe pulse. By delaying the probe pulse optically, delay times up to 12 ns can be achieved. For longer times a continuous wave (cw) probe is utilized in conjunction with a fast photomultiplier tube and fast digital sampling.

Two different pump lasers were employed for the experiments. For the ultrafast dynamics, i.e., times from tens of fs to 600 ps, a laser system consisting of a regeneratively amplified Ti:Sapphire oscillator produced pulses at a repetition rate of 5 kHz with a center wavelength of 800 nm. By adjusting the grating pulse compressor, the pulse duration could be varied from $<$70 fs to 2 ps. The shortest time scale data were recorded with the shortest pulses. For data out to 600 ps, the signal-to-noise ratio was improved by increasing the pulse duration. Increasing the pulse duration puts a frequency chirp on the pulse. However, for the nonresonant OKE experiment, a chirp does not change the data. For the slower dynamics, $t > 100$ ps, a mode-locked Q-switched cavity dumped Nd:YAG laser (1.06 μm) with a pulse length of 90 ps and a repetition rate of 1 kHz was used. Probe pulses were beam split off of the excitation pulse for measurements to 12 ns. In the Ti:Sapphire system, the probe and pump pulses were the same color. In the Nd:YAG system, the probe pulse was doubled to 532 nm. For $t > 12$ ns, the Nd:YAG pump and a 10 mW 650 nm diode laser probe were used. In all of the experiments, with the exception of certain very short time scale experiments, optical heterodyne detection (OHD) of the optical Kerr effect (OKE) signal was employed[24,25] by rotating the quarter-wave plate slightly and leaving the input and output polarizers crossed. Compared to homodyne detection, OHD detection provides better signal-to-noise ratios, and OHD detection yields a signal that is linear in the third-order dielectric susceptibility. The peak pulse power was limited to avoid damaging the sample and to assure that the homodyne component of the signal was negligible. For some very fast experiments, polarization selective transient grating OKE (TG-OKE)[32] experiments were performed because they enable the purely electronic response of the system to be eliminated from the signal.[33]

Data sets were taken on the three systems, Ti:Sapphire, Nd:YAG with delayed probe, Nd:YAG with cw probe. The scans taken over various time ranges always overlapped substantially with the time range of the next slowest scan. The extensive overlap of the scans permitted the data sets to be merged by adjusting only the relative amplitudes so the overlap regions were coincident. Great care was taken to assure that the different data sets were properly and unambiguously merged. Sufficient data were accumulated so that the signal-to-noise ratios in the data overlap regions were excellent. In many cases, it is not possible to discern in a fully merged data set where the segments were combined.

Salol (phenyl-salicylate, see structure in Fig. 1) was obtained from Aldrich. The samples were purified by vacuum distillation into a 1 cm glass cuvette for the Nd:YAG laser system and into a 1 mm glass cuvette for the Ti:Sapphire laser system. Temperature control was obtained using a constant flow cryostat or closed cycle refrigerator with temperature stability of ± 0.1 K.

Analysis of OHD-OKE data has been the subject of several publications.[34] In principle, by applying a deconvolution procedure the effect of the duration of the laser pulses can be removed from the time dependence of the signal. However, if the input pulses are significantly shorter than the observed response, which is the case in the experiments presented here, the deconvolution procedure can be omitted.

The OHD-OKE signal is proportional to the third-order dielectric susceptibility.[35] The contribution arising from molecular motions, which is of interest here, reduces to the first-

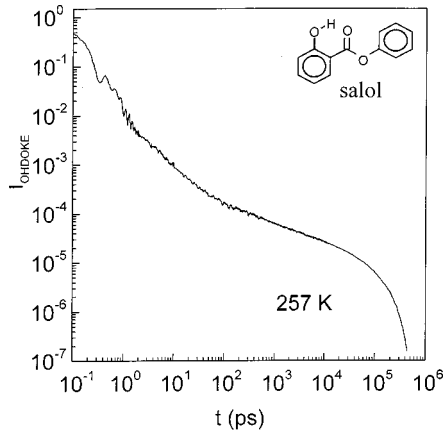

FIG. 1. Optical heterodyne detected optical Kerr effect data on a log plot for the supercooled liquid salol at 257 K from 100 fs to 0.4 μs. The inset shows the salol molecular structure. The shortest time data are the electronic response followed by oscillations that arise from the excitation of intramolecular vibrations. From ~1 ps to ~10 ns, the data consist of three regions, the critical decay, an intermediate power law, and the von Schweidler power law. At the longest times, the data decay is nearly exponential.

order dielectric tensor.[36] With the appropriate selection of polarization conditions, the imaginary part of the Fourier transform of the OHD-OKE signal,[32] $I_{\mathrm{OHDOKE}}(t)$, is proportional to data obtained from depolarized light scattering, χ''_{LS},[36]

$$\chi''_{\mathrm{LS}} \propto \mathrm{Im\,FT}\{I_{\mathrm{OHDOKE}}(t)\}. \tag{1}$$

A detailed comparison between OHD-OKE and high-resolution light-scattering data displayed excellent agreement.[36]

III. MODE-COUPLING THEORY

The data presented below will be discussed using mode-coupling theory. We will first compare the data to ideal MCT and show that the agreement is very good until T_c is approached from above. We will then examine whether the discrepancies between the data and ideal mode-coupling theory can be explained with extended mode-coupling theory. In this section, we present the necessary equations and terms required for the data analysis.

A. Ideal mode-coupling theory

Ideal MCT for supercooled liquids predicts a two-step relaxation process for the dynamics and an ideal kinetic glass transition that occurs at temperature, T_c. While MCT deals directly with density fluctuations, many experimental methods, e.g., dielectric spectroscopy[37] and dynamic light scattering,[38] probe orientational relaxation. It is assumed that the time dependence of any correlation function that is coupled to the density is similar in nature to the density–density correlation function.[6,7] However, some differences in experimental results from various experimental techniques are observed. One reason for observed deviations could be attributable to corrections to the asymptotic laws of MCT.[23,39] One important difference between molecular systems and simple liquids (spheres) is that the former have orientational degrees of freedom. MCT is derived for simple liquids. To investigate the effect of orientational degrees of freedom, molecular dynamics simulations involving translational and orientational degrees of freedom have been performed.[40,41] In general, the results of the simulations are consistent with MCT for both translational and orientational correlation functions.[41] In the analysis presented below, we will assume that results derived for the density–density correlation function can be applied to the polarizability–polarizability correlation function (orientational relaxation), which underlies the OHD-OKE measurements.

Within the two-step relaxation scenario of ideal MCT, two power laws are discussed when the theory is considered in first order. Near the ideal mode-coupling transition temperature T_c, the long time tail of the very short time dynamics (β regime) is characterized, in first order, by the critical decay law,[6,7]

$$\phi_q(t) = f_q^c + |\sigma|^{1/2} h_q \left(\frac{t}{t_\sigma}\right)^{-a}. \tag{2}$$

f_q^c denotes the critical Debye–Waller factor,[42] h_q the critical amplitude, and $t_\sigma = t_0|\sigma|^{-1/2a}$ a rescaling time determined by a microscopic time t_0. The temperature dependence is introduced by $\sigma = (T_c - T)/T_c$. MCT predicts that the exponent, a, falls in the range $0 \leqslant a \leqslant 0.395$, and it is independent of the actual observable that is coupled to the density. The initial decay of ϕ_q from the plateau value f_q^c is described in first order by another power law, the von Schweidler law,

$$\phi_q(t) = f_q^c - |\sigma|^{1/2} h_q B \left(\frac{t}{t_\sigma}\right)^{b}, \quad B > 0. \tag{3}$$

The von Schweidler power law describes the onset of the structural relaxation, which becomes an exponential or a stretched exponential at longer times.

One prediction of MCT is the relationship between the two power law exponents a and b,

$$\lambda = \frac{\Gamma^2(1-a)}{\Gamma(1-2a)} = \frac{\Gamma^2(1+b)}{\Gamma(1+2b)}, \tag{4}$$

where Γ denotes the gamma function. In the frequency domain, the region of interest is a minimum in the imaginary part of the susceptibility $\chi''(\omega)$, which is often fit to

$$\chi''(\omega) = \chi''_{\min} \frac{b(\omega/\omega_{\min})^a + a(\omega/\omega_{\min})^{-b}}{a+b}. \tag{5}$$

This expression contains both exponents. The temperature dependence of the minimum, $\chi''_{\min} = \chi''(\omega_{\min})$, can be used to determine the critical temperature, T_c. The power laws given in Eqs. (2) and (3) are the leading terms of the power law expansions[43,44] of the beta correlator,[45] which is the full solution to the kinetic equations arising in MCT. These equations are solved numerically. The power law expansions approximate the numerical solutions. More extended results of ideal MCT, including higher order terms,[44] were used to describe experimental data over larger ranges of time or frequency.[22,26,46,47] Using the higher order terms, the behavior between the limiting power laws given in Eqs. (2) and (3) can be calculated with 1% accuracy.[44] The extended forms of Eqs. (2) and (3) are, for times $t_0 < t \leqslant t_\sigma$,

$$\phi_q(t) = f_q^c + h_q|\sigma|^{1/2}[(t/t_\sigma)^{-a} - A_1(t/t_\sigma)^a + A_2(t/t_\sigma)^{3a} - A_3(t/t_\sigma)^{5a} + \cdots], \quad (6)$$

and for $t_\sigma < t \leqslant \tau_\alpha$,

$$\phi_q(t) = f_q^c + h_q|\sigma|^{1/2}[-B(t/t_\sigma)^b + (B_1/B)(t/t_\sigma)^{-b} + \cdots]. \quad (7)$$

Taking the higher order terms in the expansion of the β correlator into account, theoretical predictions can be compared to experimental data over a wide time window.

B. Extended mode-coupling theory

One weakness of ideal MCT when applied to molecular liquids arises from the predicted temperature dependence of the structural relaxation. At temperatures $T > T_c$, structural relaxation leads to a final decay of ϕ_q to zero. In ideal MCT, at T_c there is a transition from ergodic to nonergodic behavior. Below T_c, ideal MCT predicts that the system remains with $\phi_q = f_q^c$ as $t \to \infty$, i.e., structural relaxation is incomplete. The deviations from the predictions of ideal MCT are clearcut in molecular glass-forming systems in which structural relaxation is found at temperatures $T_g < T < T_c$.

In extended MCT, an additional parameter, δ, is added to the equation of motion that determines the β correlator, $G(\tau)$,[48]

$$\sigma + \lambda G^2(t) - \delta t = \frac{d}{dt}\int_0^t G(t-t')G(t')dt'. \quad (8)$$

δ is associated with hopping processes that restore ergodicity below T_c.[48–50] In a similar context, Goldstein first discussed hopping processes[51] as occurring at temperatures below the point at which ordinary diffusive processes would cease. While the idea of the hopping process was connected with density fluctuations, it may also apply to orientational relaxation if the density and orientation are coupled. A detailed treatment of an extended MCT has been presented.[48] Several derivations exist[52–55] that give the same results for the interesting transition regime between critical decay and the von Schweidler regime.[56]

IV. RESULTS AND DISCUSSION

OHD-OKE data for salol was collected for 14 temperatures between 247 and 340 K. Figure 1 shows a typical data set taken at 257 K. The data are displayed with a log plot because of the large ranges of amplitude and time spanned. Although the decay functions change significantly with temperature, some common features are clear and can be seen in Fig. 1. The initial decay is a composition of electronic and nuclear contributions.[33,57] Because of the short pulses (<70 fs) used for the earliest portion of the data, the electronic part of the OHD-OKE signal does not contribute to the signal for $t > 300$ fs. Measurements at shorter times using polarization selective TG-OKE experiments,[33] which eliminate the electronic contribution to the signal, were used to measure the decays for $t < 300$ fs and confirm that the OHD-OKE data are free of an electronic contribution for $t > 300$ fs.[33]

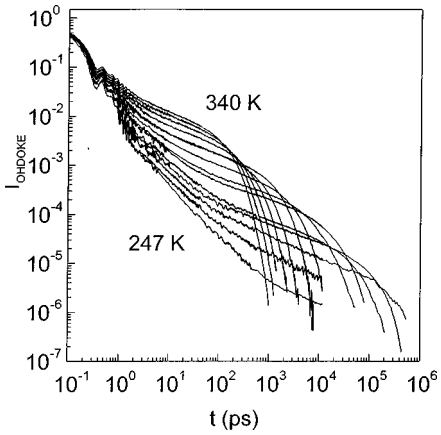

FIG. 2. The OHD-OKE signal from salol is plotted vs time on a log plot for all temperatures measured: 247, 250, 253, 257, 261, 255, 270, 280, 290, 300, 310, 320, 330, and 340 K (bottom to top). The data are scaled, $I_{OHDOKE}(t=0)=1$. At the shortest times, all of the data sets display the electronic response and intramolecular oscillations. The data sets have substantial temperature dependence.

Low-frequency internal molecular vibrations excited by stimulated Raman scattering are seen as oscillations in the signal up to ~2 ps. Because of the log time axis, the oscillations appear more closely spaced as the time gets longer. In a recent study on salol, some intramolecular degrees of freedom were identified[28] that may account for the oscillations. The structure of the signal in this time regime is complex. In addition to the oscillations, the signal decays over this period. A more detailed analysis will be given below. Once the oscillations are damped, the subsequent decay of the signal can be subdivided into different sections. Depending on the temperature, one or more power law decays can be identified. Power law decays appear as straight lines on a log plot. The final decays at long times have a stretched exponential or nearly exponential form with decay times increasing with decreasing temperature. On the log plot shown in Fig. 1, the nearly exponential decay appears as the steep descent following the more gradual decay at shorter times. All of the data sets have the same general form, but major features (power laws, final approximately exponential decays) occur on different time scales depending on the temperature. Figure 2 displays all 14 data sets. Data sets were collected from the shortest times through the final, approximately exponential, decay (not shown for the lowest temperatures).

A. Fast oscillations

Figure 3 displays the very short time portion of the data for several temperatures. The time axis is linear to make the oscillations and the decays more visible. The vertical axis is still a log scale, which distorts the appearance of the oscillations. The oscillations excited by stimulated Raman scattering are almost temperature independent in both frequency and amplitude, strongly suggesting that these oscillations arise from excitation of low-frequency internal vibrational modes of salol. The underlying decay becomes more pronounced at lower temperatures. The inset in Fig. 3 shows salol data taken at 241.4 K with a polarization selective TG-OKE experiment to separate electronic and nuclear contribu-

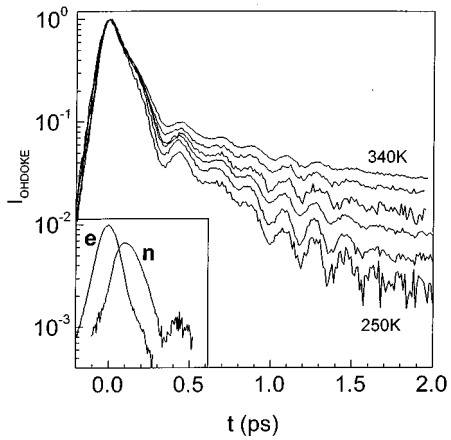

FIG. 3. The short time portions of several data sets (250, 257, 270, 290, 320, and 340 K, bottom to top) on a semi-log plot. Oscillations from intramolecular vibrations (5.7 and 4.8 THz) contribute to the OHD-OKE signal up to ~2 ps. The frequency and amplitude of the oscillations are essentially temperature independent, but the underlying decay is temperature dependent. The inset shows data taken at 241.4 K using polarization selective transient grating optical Kerr effect experiments. The choice of polarizations permits the separation of the electronic (*e*) and nuclear (*n*) contributions to the overall signal. The time axis for the inset is the same as for the main figure.

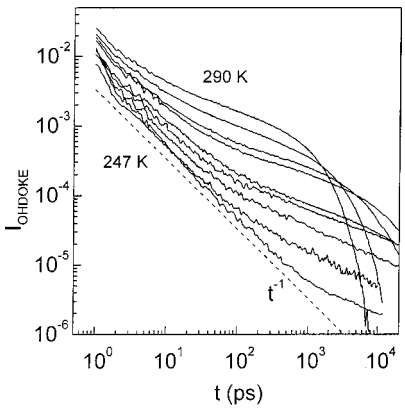

FIG. 4. The intermediate time portion of the data from ~1 ps to ~10 ns for several temperatures: 247, 250, 253, 257, 261, 266, 270, 280, and 290 K (bottom to top). The data are scaled, $I_{OHDOKE}(t=0)=1$. The data appear to be a power law at intermediate times. This can be seen most clearly in the $T=247$ K data, where the intermediate power law span is $\sim 2 \leqslant t \leqslant \sim 500$ ps. The dashed line is a plot of t^{-1} as an aid to the eye.

tions to the signal.[33] While the OHD-OKE experiment gives a signal linear in the induced polarization, the TG-OKE experiment produces a signal proportional to the absolute value squared of the polarization. The time axis is the same as in the main figure. The electronic signal (e) reflects the pulse shape. The shift of the nuclear signal from the electronic signal is real and arises because of the time required for orientational displacement to occur following the impulsive excitation of the sample. The inset demonstrates that data at longer times are not influenced by the electronic contribution to the signal.

The oscillations can be decomposed into two components, which differ in frequency, amplitude, and decay time. The corresponding values obtained by a fitting procedure are shown in Table I. The data were fit to two exponentially damped sinusoids and an additional slowly decaying stretched exponential. The stretched exponential was used only to model the underlying decay in the fit to the oscillations. It was not used in the subsequent MCT data analysis. The two frequencies are 5.7 THz (190 cm^{-1}) and 4.8 THz (160 cm^{-1}). The high frequencies indicate that the oscillations arise from intramolecular modes. To confirm that the oscillations are intramolecular, experiments were performed in a solution of 5 mol% salol in CCl_4 at room temperature. The same oscillations were found, verifying that the oscillations are from intramolecular vibrations of salol.

TABLE I. The initial oscillatory part of the OKE signal can be decomposed in two components that differ in frequency, amplitude, and decay time.

	Relative amplitude	Frequency	Decay time
1	(25±5)%	(5.7±0.1) THz	(2.1±0.3) ps
2	(75±5)%	(4.8±0.1) THz	(2.6±0.3) ps

B. The intermediate time scale data

Figure 4 displays some of the data shown in Fig. 2 but on an expanded time scale to emphasize the intermediate time regime. Also shown in Fig. 4 is a plot of t^{-1} (dashed line) as an aid to the eye. At times just prior to the stretched exponential (long time) portion of the decay, all of the decays display a power law behavior. This power law, the von Schweidler region in the MCT, can be seen in Fig. 4 most clearly in the intermediate temperature data. At short times, $t<2$ ps, another power law is observed. This can be seen most clearly in the low-temperature curves in Fig. 4, although the small range over which this power law can be distinguished from the shortest time scale part of the signal makes direct analysis difficult (see below). In addition to the short time critical decay (attributed to the fast β process) power law and the long time von Schweidler power law, we observe a substantial region between these that has the appearance of a power law, which will be referred to as the intermediate power law. The intermediate power law can be seen most clearly in Fig. 4 in the low-temperature curves. At 247 K, it extends from $t>2$ up to ~500 ps. Comparison of this curve to the t^{-1} line shows that the data are $\sim t^{-1}$.

To analyze the power laws quantitatively, several procedures were employed. The derivatives, $d \log I_{OHDOKE}/d \log t$, of the salol data were plotted. A power law decay results in a horizontal line, and the exponent is the *y* axis intercept. We used this procedure to test if power laws are present. Noise in the original data is amplified by taking the derivative; therefore, the procedure could only be used for $T \geqslant 253$ K. Two different power law regimes were clearly revealed. The exponent of the fast one changes with temperature. The exponent of the slower one remains almost constant over the entire temperature regime.

For a quantitative analysis, the I_{OHDOKE} data were fit to several power laws. The OHD-OKE experiment measures the impulse response function. The impulse response function is the time derivative of the associated correlation function. To compare to exponents calculated for the density–density correlation function with MCT, the following

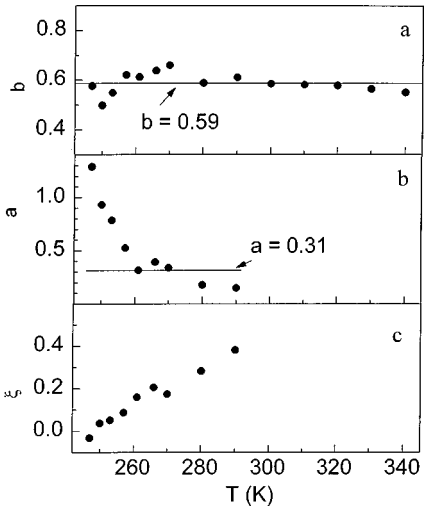

FIG. 5. The power law exponents, x, found in the experimental data are converted to $b=1+x$ and $a=-1-x$, where a and b are given in Eqs. (2) and (3), and the relationship between them is given in Eq. (4). In addition, the intermediate power law exponent is $\xi=1+x$. (a) The slowest power law, the von Schweidler power law, can be measured over the entire temperature regime with an almost constant value of the exponent $b=0.59$. (b) The fastest power law, attributed to the critical decay, has a value of the exponent $a\cong 0.3$ near the mode-coupling theory T_c in accord with Eq. (4). Below T_c, the exponent a is highly temperature dependent. Well above T_c, it also appears to be temperature dependent, but its value is difficult to measure at higher temperatures. (c) The intermediate power law exponent, ξ. A value of $\xi\cong 0$ corresponds to an experimental intermediate power law of $\sim t^{-1}$ (see Fig. 4).

identifications are made. We associate the fast and the slow power laws with the critical decay and the von Schweidler decay, respectively. The exponents, x, found in the experimental data are converted to the parameters used in the correlation functions via $b=1+x$ and $a=-1-x$, where a and b are given in Eqs. (2) and (3), and their relationship is given in Eq. (4). At the highest temperatures, only the von Schweidler power law can be clearly identified; at lower temperature, $T\leqslant 290$ K, the exponents of all three power laws can be determined.

Figure 5(a) displays the exponents for the von Schweidler power law. Within experimental error, b is temperature independent. Its value, obtained by averaging over all temperatures, is $b=0.59$, which is in accord with light-scattering experiments.[16] From Eq. (4), this value of b gives $\lambda=0.73$.

To analyze the contributions from relaxation to the OHD-OKE signal at short times, $t<2$ ps, it was necessary to remove the oscillations in the data. To do this, the data were Fourier transformed into the frequency domain, and the resulting frequency domain data were numerically filtered using a Gaussian shape for the peaks occurring at the frequencies of the oscillations. The filtered data were back Fourier transformed. This procedure worked well for $t\geqslant 1$ ps, but at shorter times, some oscillatory components remained. We therefore restrict our data analysis to times $t\geqslant 1$ ps. To assure that removing the oscillations from the signal has no affect on the remaining relaxation curve, several experiments at one temperature were performed with significantly longer pulse lengths. The additional data were taken with 160 fs pulses. These pulses are too long to excite the internal vibrations. The data taken with the longer pulses had no oscillations and agreed perfectly with the short pulse decays that had the oscillations removed by the Fourier transform method.

As will be discussed subsequently, the slope of the data changes at ~ 2 ps. Breaking the time dependence into regions represented by power laws is a first-order description of the data. The data will be reconsidered including higher order terms in ideal MCT. However, obtaining the power law exponents for the critical decay (fast β process) and the von Schweidler decay provides insight into the temperature-dependent behavior of the system. The time range available to determine the critical decay exponent is very limited, $1\leqslant t\leqslant 2$ ps. While it is somewhat arbitrary, we have chosen a power law to characterize the data in this range so that we can compare with quantitative predictions of MCT close to the MCT transition temperature, T_c. (For salol, $T_c\cong 257$ K;[16,58,59] there is a significant error bar on this value.) Figure 5(b) displays the exponent a [Eq. (2)]. The value is temperature dependent, particularly below T_c. It is noteworthy that for $T_c<T<T_c+10$ K, we find an exponent $a\approx 0.3$,[39] which is in accord with $b=0.59$ and $\lambda=0.73$ via Eq. (4). Below T_c, a is highly temperature dependent and increases to 1.3 at 247 K. At temperatures well above T_c, a appears to decrease with increasing temperature, but its value is difficult to measure accurately in this temperature range.

Between the critical decay and von Schweidler power laws, there is a significant range of the data that has the appearance of another power law, the intermediate power law. At 290 K, the experimental value of the intermediate power law exponent is ~ -0.6, and the exponent becomes progressively more negative as the temperature decreases. While at the high temperatures, separating the components of the decays is difficult, at lower temperatures the three different power laws can be distinguished readily. As can be seen in Fig. 4, the intermediate power law exponent is ~ -1 at 247 K, which is below T_c. The crossover from the fast decay to the intermediate power law is almost temperature independent and located at ~ 2 ps. The crossover from the intermediate to the slow power law shifts from about 10 ps at 290 K to ~ 500 ps at 247 K. The temperature dependence of the intermediate power law exponent is shown in Fig. 5(c) as $\xi=1+x$, where x is the experimentally measured exponent. $\xi=\sim 0$ corresponds to an observed exponent of ~ -1.

C. Comparison to ideal MCT including higher order terms

In the previous section, the data were discussed in terms of three power laws, the critical decay at short time, the von Schweidler decay at longer times, and the region between these two power laws, which was modeled as the intermediate power law. The intermediate power law spans a broader range of times as the temperature is decreased, and it is $\sim t^{-1}$ below T_c (see Figs. 4 and 5). To examine the time range covering the critical decay through the von Schweidler decay quantitatively, it is necessary to go beyond first order in the description of ideal MCT. The critical decay power law and the von Schweidler power law [Eqs. (2) and (3)] are

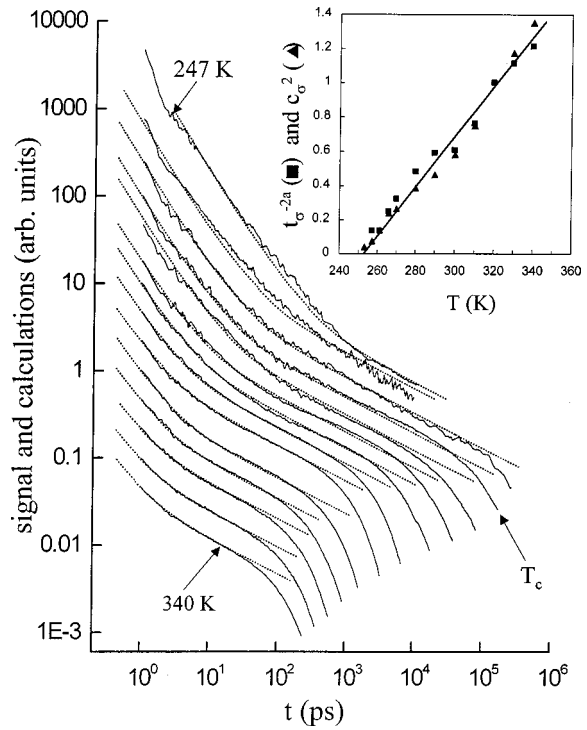

FIG. 6. The salol data compared to the master curve calculations (β correlator), Eqs. (6) and (7), predicted by ideal mode-coupling theory using $\lambda=0.73$ from Eq. (4) for $b=0.59$. The curves are for temperatures (top to bottom) 247, 250, 253, 257, 261, 266, 270, 280, 290, 300, 310, 320, 330, and 340 K. For temperatures above T_c, the agreement between the predictions of ideal MCT and the data is remarkable. The inset displays the so-called rectification diagrams. MCT predicts that the quantities t_σ^{-2a} and c_σ^2, where c_σ is the amplitude of the data, should depend linearly on T, and the intersection of the lines with the abscissa gives T_c. Both types of data display the predicted dependence and give $T_c=252$ K. Below T_c, the time-dependent data do not have the shape of the master curve.

the leading terms of Eqs. (6) and (7). A quantitative comparison between the data and ideal MCT can be performed by solving the MCT equation of motion to obtain the beta correlator[45] either numerically or by using power law expansions with the appropriate coefficients.[43,44] Here we employ the power law expansions given in Eqs. (6) and (7).

Equations (6) and (7) combine to provide a master curve. Once λ is obtained from experiment, all of the coefficients in Eqs. (6) and (7) are known.[43,44] There are no adjustable parameters in Eqs. (6) and (7). Equation (6) goes over to Eq. (7) at t_σ, and the time axis is scaled by $1/t_\sigma$. At sufficiently long time, the master curve goes over to a form that is approximately a stretched exponential with time constant $\tau_\alpha \propto |\sigma|^{-\gamma}$ with $\gamma=(1/2a)+(1/2b)$. The long time, α relaxation, portions of the data will be discussed below.

Figure 6 displays the salol data compared to the master curve calculations. The curves have been offset on the vertical axis for clarity of presentation. The amplitudes of the curves are discussed below. The long time scale α portions of the calculations have been omitted (see Fig. 10). To determine λ, we use the experimental value of the exponent b, since it could be determined with more accuracy than the exponent a. For $b=0.59$, from Eq. (4), $\lambda=0.73$. The tabulated expansion coefficients[44] were used; only t_σ (discussed below) was adjusted for each temperature to obtain a best agreement. Above T_c, the shape of the master curve shows outstanding agreement with the data over the full range of times. The ability of ideal mode-coupling theory to reproduce the functional form of the data is remarkable.

In addition to the temperature-dependent shapes of the master curves, ideal MCT also predicts the temperature dependence of t_σ and c_σ, the amplitude of the curves. The t_σ were obtained from the comparison of the calculated master curves to the data. The c_σ were obtained in the following manner. Around $t=0$, the OHD-OKE signal is completely dominated by the electronic response of the system. Therefore, the size of the $t=0$ peak can be used to normalize the data at each temperature even though the instrumental settings may change from one temperature to another. c_σ is the amplitude of the $I_{\text{OHD-OKE}}(t=t_\sigma)\cdot t_\sigma$ scaled by $I_{\text{OHD-OKE}}(t=0)$.

MCT predicts that the quantities t_σ^{-2a} and c_σ^2 should depend linearly on T. The intersections of these lines with the abscissa is T_c, the mode-coupling transition temperature. The inset in Fig. 6 displays the so-called rectification diagrams, where t_σ^{-2a} and c_σ^2 are plotted vs temperature. A is taken to be 0.32 in accord with $\lambda=0.73$. Since the values of c_σ^2 are relative, they were scaled to use the same vertical axis at t_σ^{-2a} to make possible a direct comparison. As can be seen in the inset, both types of data fall on the same line and give a value of $T_c=252$ K with an error bar estimated to be ± 4 K. This value is consistent with previous estimates of T_c that average to 257 K[16,58,59] with an error of approximately ± 6 K. (As discussed below, the rectification diagram for τ_α gives $T_c=255$ K.) The fact that the t_σ data and the c_σ data as well as the master curve data obey the predictions of ideal MCT is truly noteworthy. While t_σ was varied to obtain the calculated master curves, the resulting values of t_σ obey the MCT predictions.

However, close to and below T_c, it can be seen that the master curve data in Fig. 6 do not have the same form as the calculated master curves, even with the adjustment of t_σ. Furthermore, in ideal MCT, as T_c is approached, the time scaling t_σ goes to infinity. Ideal MCT predicts an ergodic to nonergodic transition at T_c. The data should plateau ($t_\sigma \rightarrow \infty$), and complete structural relaxation should cease at T_c. These predictions are not in accord with the data.

While the ideal MCT master curve does a very good job of describing the data above T_c, it cannot describe the data below T_c. As pointed out above, the data between the critical decay and the von Schweidler decay have the appearance of a power law with a temperature-dependent exponent. Below T_c, ideal MCT predicts a plateau following the critical decay.

The impulse response function, measured by the OHD-OKE experiments, is proportional to the time derivative of the correlation function. Since we observe a functional form that has the appearance of a power law decay in what should be the plateau region, instead of describing the plateau by a constant, we will employ a heuristic model for the purposes of discussion, i.e.,

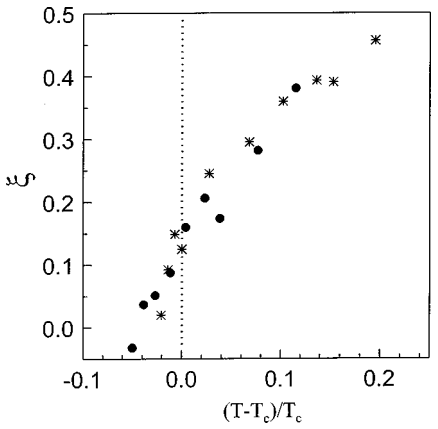

FIG. 7. The correlation function exponent ξ [Eq. (9)] of the intermediate power law data is plotted versus a reduced temperature for two samples salol (●) ($T_c=257$ K) and ortho-terphenyl (*) ($T_c=290$ K). (Refs. 26 and 60). Within experimental error, the two liquids have the identical temperature dependences of ξ. Slightly below the literature value of T_c, $\xi\sim 0$, which corresponds to a power law $\sim t^{-1}$ in the data (see Fig. 4). From Eq. (9), $\xi\sim 0$ implies that the correlation function is approximately a plateau.

$$\phi(t)=f_q^c\left(2-\left(\frac{t}{t_\xi}\right)^{\xi}\right). \tag{9}$$

t_ξ is a rescaling time. In this heuristic description, for $T\leqslant T_c$, the ideal MCT plateau would correspond to $\xi=0$, and Eq. (9) reduces to $\phi(t)=f_q^c$. Since the experimental data are related to the derivative of Eq. (9), for $\xi\sim 0$, the signal will decay as $\sim t^{-1}$.

As shown in Fig. 5(c), the exponent, ξ, progresses smoothly to ~ 0 as the temperature is decreased. This behavior does not seem to be peculiar to salol. In Fig. 7 the temperature-dependent exponents, ξ, are plotted for salol and ortho-terphenyl ($T_c=290$ K) versus a reduced temperature. (The full details of the experiments on ortho-terphenyl will be published subsequently.[60]) Within experimental error, the two liquids display identical temperature dependences. For $T>T_c$, $\xi>0$. ξ decreases with temperature, and below T_c, becomes ~ 0. $\xi\cong 0$ in Eq. (9) corresponds to an almost constant correlation function (the ''plateau'' region) between the critical decay and the von Schweidler regime.

D. Extended MCT analysis

In ideal MCT, structural relaxation occurs only above T_c. The parameter, λ, determines the shape of the β-relaxation function via the power law exponents a and b. A change in temperature shifts the time scale of the β-relaxation function but does not affect its shape. In extended MCT [Eq. (8)], the additional hopping parameter, δ, affects the shape of the relaxation function.[48] In extended MCT, the shape of the time-dependent function is determined by three parameters, $\sigma(T)$, λ, and δ. δ and σ can be combined with t_0 to give $\hat{\delta}=t_0\delta/\sigma$, reflecting the scaling behavior of Eq. (8). Then, $\hat{\delta}$ and λ determine the shape of the β-relaxation function. $\hat{\delta}=0$ corresponds to ideal MCT.

Figure 8 compares experimental data taken below T_c with extended MCT calculations.[61] The calculations were performed with $\lambda=0.73$ for three cases: (a) $T>T_c$, $\hat{\delta}=0$ (dotted line), (b) $T\approx T_c$, $\hat{\delta}\gg 1$ (dashed line), and (c) $T<T_c$, $\hat{\delta}\ll 1$ (dashed-dotted line). The $\hat{\delta}\gg 1$ case has substantial hopping (large δ) with a small σ, i.e., T is near T_c. The $\hat{\delta}\ll 1$ case has δ less than a certain value (relatively small δ) and T well below T_c. Many calculations were performed that spanned a wide range of δ and σ. The three cases presented here represent limiting situations and all the other calculations produce curves that fall between those shown here. The shape of the curves calculated for $\hat{\delta}\gg 1$ are identical for all temperatures above and below T_c. As discussed in the previous section, the experimental data are well described by ideal MCT above T_c with $\lambda=0.73$.

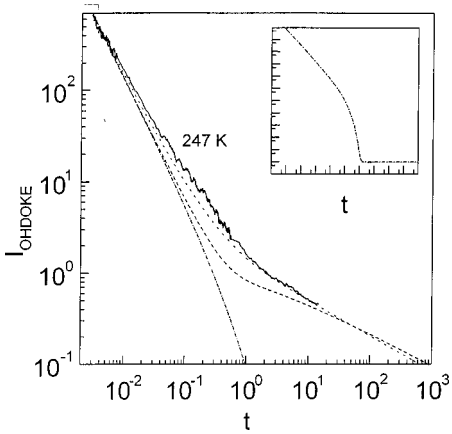

FIG. 8. Experimental data at 247 K and extended MCT calculations [Eq. (8)] with $\lambda=0.72$ for three cases: (a) $\hat{\delta}=0$, no hopping (dotted line), (b) $\hat{\delta}\gg 1$, substantial hopping (dashed line), and (c) $\hat{\delta}\ll 1$, relatively little hopping (dashed-dotted line). Many calculations were performed that cover a wide range of parameters. All calculations produce curves that fall between those shown. The calculations show that extended MCT cannot account for the shape of the experimental data below T_c. The impulse response function for case (c) ($\hat{\delta}\ll 1$) shows an additional feature following the critical decay; the relaxation first slows down and then speeds up again at longer times. A typical example is plotted in the inset with $\hat{\delta}=10^{-6}$. The vertical position of the plateau, which appears after the downward bend, depends on the value of $\hat{\delta}$.

The transition region between the critical decay and the von Schweidler decay corresponds in the frequency domain to the minimum in the susceptibility $\chi''(\omega)$. In the experiments, this region is becoming broader as the temperature decreases. The ''intermediate power law'' has a wider time span as the temperature is lowered. In contrast, extended MCT predicts the opposite behavior; the transition becomes sharper with decreasing temperature. The impulse response function (time derivative of the correlation function) for case (c) ($\hat{\delta}\ll 1$) shows an additional feature in the transition regime, i.e., where in ideal MCT the crossover from the critical decay to the von Schweidler decay occurs. Following the critical decay, the relaxation first slows down and then speeds up again at longer times. A typical example for case (c) is plotted in the inset of Fig. 8 with $\hat{\delta}=10^{-6}$. While in case (b), $\hat{\delta}\gg 1$ is sufficient to determine the shape of the decay, in case (c), the vertical position of the plateau, which appears after the downward bend, depends on the value of $\hat{\delta}$. As $\hat{\delta}$ becomes smaller, the location of the plateau is lowered. At longer times, not shown in the inset, the curve turns down

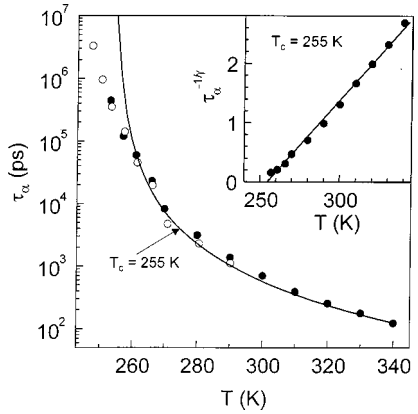

FIG. 9. The long time decay time τ_α (filled circles) and additional data reported previously (Ref. 29) (open circles). The solid line is calculated with ideal MCT using Eqs. (11) and (12) with $T_c = 255$ K. The inset shows the rectification diagram for τ_α, i.e., $\tau_\alpha^{-1/\gamma}$ vs T with $\gamma = 2.4$. Extrapolating $\tau_\alpha^{-1/\gamma}$ to the intersection of the line with the abscissa gives $T_c = 255$ K.

again, becoming a power law decay dominated by the hopping process. In the frequency domain, the downward bend to an almost vertical decay corresponds to the so-called ''knee.'' (It should be noted that in recent light-scattering experiments, the knee, which had been reported previously, was not observed, and its previous reports were attributed to an artifact in earlier experiments.[62–64])

The calculations in Fig. 8 show that extended MCT cannot account for the shape of the experimental data below T_c. Independent of the choice of $\hat{\delta}$, the decays calculated with extended MCT fall too quickly. In fact, the curve that comes closest to the data is for $\hat{\delta} = 0$, i.e., ideal MCT, which does not apply below T_c. As shown in Fig. 7, for both salol and ortho-terphenyl, there is a smooth progression of the data from well above T_c to below T_c. Ideal MCT does an excellent job of describing the data above T_c. Extended MCT is not able to reproduce the data at and below T_c using either a small or large hopping parameter. Clearly, extended MCT is in accord with the data in the sense that it eliminates the plateau predicted by ideal MCT. It is possible that an alternative extension of MCT with some type of hopping could account for the data.

E. Structural relaxation

The portions of the experimental relaxation curves with the strongest temperature dependences are at the longest times (see Figs. 1 and 2). The long time component of the decays corresponds to the structural relaxation (α-process). Figure 9 displays the decay times, τ_α, obtained by fitting the data at long times to[60]

$$f \propto t^p \exp(-t/\tau_\alpha). \tag{10}$$

Also plotted are the decay times from long time data previously obtained on salol.[29] The decay times have the temperature dependence typical of fragile supercooled liquids. The decay slows substantially as the temperature is reduced, going from ~100 ps at the highest temperature to several μs at the lowest temperature.

Figure 9 contains the calculated curve based on the prediction of ideal MCT, i.e.,

$$\tau_\alpha \propto |\sigma|^{-\gamma}, \tag{11}$$

with

$$\gamma = \frac{1}{2a} + \frac{1}{2b}. \tag{12}$$

Using $b = 0.59$ (see Fig. 5) and the corresponding value of a, $\gamma = 2.4$. The inset displays the rectification diagram for τ_α. Extrapolating $\tau_\alpha^{-1/\gamma}$ linearly to the intersection with the abscissa yields $T_c = 255$ K. This value is within experimental error of the value determined from the inset of Fig. 6 and of the values reported previously.[16,58,59] The ideal MCT calculated curve (solid line in the main body of the figure) with $T_c = 255$ K does an excellent job of reproducing the data with no adjustable parameters down to $\sim T_c$. Clearly, the prediction of ideal MCT of vanishing structural relaxation at T_c, a temperature well above the laboratory T_g, is not fulfilled. Below T_c the α-process continues to slow, as can be seen in Fig. 9. Nonetheless, above T_c, ideal MCT does a notable job of describing the data. With a single value of the von Schweidler power law exponent b, obtained from the experimental data (Fig. 5), ideal MCT is able to reproduce the data through the predictions of the short through intermediate time scale master curve (Fig. 6) and the long time decay parameter, τ_α, from ~1 ps to μs.

The OHD-OKE experiments measure the time derivative of the polarizability–polarizability correlation function (orientational relaxation). MCT describes the density–density correlation function. The agreement between the predictions of MCT and the data supports the assumption that the behavior of these two correlation functions is closely related.

F. The boson peak

A feature that is observed in many scattering experiments on supercooled liquids is referred to as the boson peak.[65–68] This feature also appears in the present data, but it can be seen more readily by a frequency domain representation of the susceptibility, $\chi''(\nu)$, shown in Fig. 10. The oscillations in the time domain data at very short times, arising from the intramolecular vibrations (Figs. 1–3), are visible in Fig. 10 as two peaks at 4.8 and 5.7 THz. Two features dominate the frequency domain data at lower frequencies. The microscopic peak, to which the data are normalized, shows significant temperature dependence. It shifts from ~1.5 THz at 340 K to ~1.9 THz at 247 K. The inset shows the peak position as a function of temperature.

At ~0.5 THz, an enhancement in the susceptibility can be found, which is attributed to the boson peak.[65–68] In specific heat measurements, the boson peak shows up as an excess contribution.[69] Several explanations for the boson peak have been proposed;[70–72] however, a consensus about its microscopic origin is still missing.

V. CONCLUDING REMARKS

In this paper, detailed time domain experiments have been used to study the dynamics in the supercooled liquid,

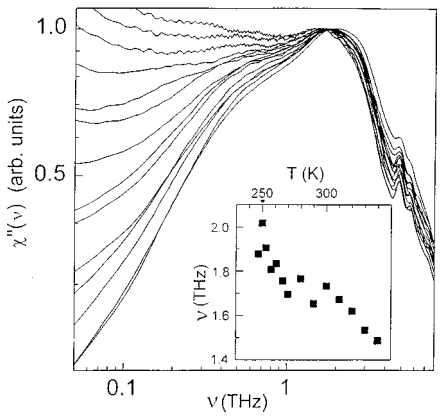

FIG. 10. Data from Fig. 2 are shown in the frequency domain for high frequencies. The intramolecular vibrational frequencies appear as peaks at 5.7 and 4.8 THz and are temperature independent. The data are normalized at the maximum of the microscopic peak, which shifts from ~1.5 THz at 340 K to ~1.9 THz at 247 K (see inset). At lower frequencies, the boson peak shows up as an enhancement in the susceptibility around 0.5 THz.

salol. The experiments employed optical heterodyne detected optical Kerr effect and transient grating optical Kerr measurements, which were able to span a time range from ~100 fs to ~1 μs. The experiments were conducted from 340 K, well above the mode-coupling theory T_c down to 247 K, below T_c. At the shortest times, high-frequency oscillations are observed to arise from intramolecular vibrations of salol. At longer times, the data have the appearance of three power laws. The power law on the shortest time scale is the critical decay (fast β process). The power law on the longest time scale is the von Schweidler decay. Between these is a region that increases in time scale from 10 ps at 340 K to 500 ps at 247 K (see Fig. 4), which we call the intermediate power law. At times longer than the von Schweidler power law, the data decay almost exponentially. The long time decay is the α-process, i.e., complete orientational relaxation.

The experimental data are compared to the predictions of ideal mode-coupling theory and extended mode-coupling theory. For temperatures above T_c, ideal MCT does a truly remarkable job of describing the data. Using the experimental determination of the von Schweidler power law exponent, b (see Fig. 5), ideal MCT predicts master curves with temperature-dependent time scaling that are able to do an accurate job of reproducing the temperature-dependent data in the time range spanned by the three power laws mentioned above (see Fig. 6). The master curves can be calculated without recourse to adjustable parameters other than the amplitude of the overall curves. The scaling time, t_σ, and the amplitude, c_σ, also conform to the prediction of ideal MCT (see inset Fig. 6), i.e., t_σ^{-2a} and c_σ^2 fall on a line and yield a consistent value of $T_c = 252$ K. In addition, using the exponent b as the experimental input, ideal MCT reproduces the temperature dependence of τ_a, the decay constant for the long time scale α-process, and $\tau_\alpha^{-1/\gamma}$ vs temperature fall on a line as predicted, yielding $T_c = 255$ K, a consistent value within experimental error.

The data on all time scales make a continuous progression with temperature as the temperature is decreased below T_c, in contrast to the predictions of ideal MCT. The intermediate power law, which above T_c is a portion of the master curve, goes as $\sim t^{-1}$ below T_c. The optical Kerr effect experiment measures the impulse response function, which is the derivative of the polarizability–polarizability correlation function. In essence, the experiment measures orientational relaxation in the same manner as light scattering does in the frequency domain. MCT describes the density–density correlation function. Because density and orientational fluctuations are intimately connected, it is assumed that the predictions of MCT also apply to the orientational correlation function. The excellent agreement between the data and ideal MCT above T_c is an indication that this assumption is correct. Following the critical decay, ideal MCT predicts that the correlation function will be a plateau at T_c, i.e., complete structural relaxation will not occur. It is interesting to note that if the correlation function is a power law with exponent ~0 rather than a plateau, then the time derivative will be a power law with exponent ~ -1, as observed. The intermediate power law is a useful phenomenological description because it permits the data to be described in a consistent manner above and below T_c. Figure 7 shows that the behavior of the intermediate power law is the same in salol and ortho-terphenyl.

Extended mode-coupling theory was developed to account for the structural relaxation that is observed in supercooled liquids below T_c down to the glass transition. A hopping mechanism is added to the equations of motion of ideal MCT. However, as shown in Fig. 8, extended MCT cannot reproduce the experimentally observed functional form of the data below T_c. Regardless of the choice of the hopping parameter, extended MCT predicts decays that are too steep in the time range from the critical decay to the von Schweidler power law.

The experiments presented in this paper provide a detailed view of dynamics in a supercooled liquid. The comparisons to theory show that ideal MCT provides an excellent description of the temperature-dependent dynamics above T_c, but extended MCT is not yet able to capture the nature of the dynamics at or below T_c.

ACKNOWLEDGMENTS

We would like to thank Professor H. C. Andersen, Department of Chemistry, Stanford University, for informative conversations pertaining to this work. We thank A. Latz, Department of Physics, University of Mainz, for providing the software used to perform the extended MCT calculations and for fruitful discussions. We thank W. Götze for many helpful suggestions concerning the data analysis. This work was made possible by a grant from the National Science Foundation (DMR-0088942). G. Hinze would like to thank the Alexander von Humboldt Foundation for partial support.

[1] C. A. Angell, J. Phys. Chem. Solids **49**, 863 (1988).
[2] I. Chang and H. Sillescu, J. Phys. Chem. **101**, 8794 (1997).
[3] W. Götze and L. Sjögren, Rep. Prog. Phys. **55**, 241 (1992).
[4] G. Hinze and H. Sillescu, J. Chem. Phys. **104**, 314 (1996).
[5] M. D. Ediger, C. A. Angell, and S. R. Nagel, J. Phys. Chem. **100**, 13200 (1996).
[6] W. Götze and L. Sjögren, Rep. Prog. Phys. **55**, 241 (1992).
[7] W. Götze, J. Phys.: Condens. Matter **11**, A1 (1999).

[8] K. L. Ngai, E. Riande, and G. B. Wright, J. Non-Cryst. Solids **172–174**, 1 (1994).
[9] K. L. Ngai and E. Riande, J. Non-Cryst. Solids **235–237**, 1 (1998).
[10] M. Giordano, D. Leponini, and M. Tosi, J. Phys.: Condens. Matter **11**, A1 (1999).
[11] P. Lunkenheimer, A. Pimenov, M. Dressel, Y. G. Goncharov, R. Böhmer, and A. Loidl, Phys. Rev. Lett. **77**, 318 (1996).
[12] U. Schneider, P. Lunkenheimer, R. Brand, and A. Loidl, Phys. Rev. E **59**, 6924 (1999).
[13] G. Li, W. M. Du, X. K. Chen, and H. Z. Cummins, Phys. Rev. A **45**, 3867 (1992).
[14] H. Z. Cummins, G. Li, W. Du, Y. H. Hwang, and G. Q. Shen, Prog. Theor. Phys. Suppl. **126**, 21 (1997).
[15] R. Bergmann, L. Börjesson, L. M. Torell, and A. Fontana, Phys. Rev. B **56**, 11619 (1997).
[16] G. Li, M. Du, A. Sakai, and H. Z. Cummins, Phys. Rev. A **46**, 3343 (1992).
[17] J. Wuttke and M. Goldammer (in preparation).
[18] R. Torre, P. Bartolini, and R. M. Pick, Phys. Rev. E **57**, 1912 (1998).
[19] A. Sengupta and M. D. Fayer, J. Chem. Phys. **100**, 1673 (1994).
[20] W. Petry, E. Bartsch, F. Fujara, M. Kiebel, H. Sillescu, and B. Farago, Z. Phys. B: Condens. Matter **83**, 175 (1991); A. Arbe, D. Richter, J. Colmenero, and B. Farago, Phys. Rev. E **54**, 3853 (1996).
[21] M. Kiebel, E. Bartsch, O. Debus, F. Fujara, W. Petry, and H. Sillescu, Phys. Rev. B **45**, 10301 (1992).
[22] A. Tölle, H. Schober, J. Wuttke, and F. Fujara, Phys. Rev. E **56**, 809 (1997).
[23] T. Franosch, M. Fuchs, W. Goetze, M. R. Mayr, and A. P. Singh, Phys. Rev. E **55**, 7153 (1997).
[24] D. McMorrow, W. T. Lotshaw, and G. Kenney-Wallace, IEEE J. Quantum Electron. **24**, 443 (1988).
[25] D. McMorrow and W. T. Lotshaw, J. Phys. Chem. **95**, 10395 (1991).
[26] G. Hinze, R. Francis, and M. D. Fayer, Phys. Rev. Lett. **84**, 2437 (2000).
[27] R. Boehmer, K. L. Ngai, C. A. Angell, and D. J. Plazek, J. Chem. Phys. **99**, 4201 (1993).
[28] A. Doess, G. Hinze, R. Boehmer, and H. Sillescu, J. Chem. Phys. **112**, 5884 (2000).
[29] G. Hinze, R. Francis, and M. D. Fayer, J. Chem. Phys. **111**, 2710 (1999).
[30] S. Ruhman, L. R. Williams, A. G. Joly, B. Kohler, and K. A. Nelson, J. Phys. Chem. **91**, 2237 (1987).
[31] F. W. Deeg, J. J. Stankus, S. R. Greenfield, V. J. Newell, and M. D. Fayer, J. Chem. Phys. **90**, 6893 (1989).
[32] OHD-OKE and OHD-RIKE are used synonymously in literature.
[33] F. W. Deeg and M. D. Fayer, J. Chem. Phys. **91**, 2269 (1989).
[34] M. Cho, M. Du, N. F. Scherer, G. R. Fleming, and S. Mukamel, J. Chem. Phys. **99**, 2410 (1993).
[35] P. P. Ho and R. R. Alfano, Phys. Rev. A **20**, 2170 (1979).
[36] S. Kinoshita, Y. Kai, M. Yamaguchi, and T. Yagi, Phys. Rev. Lett. **75**, 148 (1995).
[37] C. J. F. Böttcher and P. Bordewijk, *Theory of Electric Polarization* (Elsevier, Amsterdam, 1992).
[38] B. J. Berne and R. Pecora, *Dynamical Light Scattering* (R. E. Krieger, Malabar, Florida, 1990).
[39] F. Sciortino and P. Tartaglia, J. Phys.: Condens. Matter **11**, 261 (1999).
[40] S. Kämmerer, W. Kob, and R. Schilling, Phys. Rev. E **56**, 5450 (1997).
[41] S. Kämmerer, W. Kob, and R. Schilling, Phys. Rev. E **58**, 2141 (1998).
[42] S. W. Lovesey, *Theory of Neutron Scattering from Condensed Matter* (Clarendon, Oxford, 1984).
[43] E. Bartsch, Transp. Theory Stat. Phys. **24**, 1125 (1995).
[44] W. Götze, J. Phys.: Condens. Matter **2**, 8485 (1990).
[45] G. Li, G. M. Fuchs, W. M. Du, A. Latz, N. J. Tao, J. Hernandez, W. Götze, and H. Z. Cummins, J. Non-Cryst. Solids **172**, 43 (1994).
[46] J. Wuttke, M. Kiebel, E. Bartsch, F. Fujara, W. Petry, and H. Sillescu, Z. Phys. B: Condens. Matter **91**, 357 (1993).
[47] E. Bartsch, V. Frenz, J. Baschnagel, W. Schaertl, and H. Sillescu, J. Chem. Phys. **106**, 3743 (1997).
[48] M. Fuchs, W. Götze, S. Hildebrand, and A. Latz, J. Phys.: Condens. Matter **4**, 7709 (1992).
[49] H. Z. Cummins, W. M. Du, M. Fuchs, W. Götze, S. Hildebrand, A. Latz, G. Li, and N. J. Tao, Phys. Rev. E **47**, 4223 (1993).
[50] W. M. Du, G. Li, H. Z. Cummins, M. Fuchs, J. Toulouse, and L. A. Knauss, Phys. Rev. E **49**, 2192 (1994).
[51] M. Goldstein, J. Chem. Phys. **51**, 3728 (1969).
[52] S. P. Das and G. F. Mazenko, Phys. Rev. A **34**, 2265 (1986).
[53] W. Götze and L. Sjögren, Z. Phys. B: Condens. Matter **65**, 415 (1987).
[54] R. Schmitz, J. W. Dufty, and P. De, Phys. Rev. Lett. **71**, 2066 (1993).
[55] C. Z.-W. Liu and I. Oppenheim, Physica A **235**, 369 (1997).
[56] A. Latz private communication (2000).
[57] W. T. Lotshaw, D. McMorrow, C. Kalpouzos, and G. A. Kenney-Wallace, Chem. Phys. Lett. **136**, 323 (1987).
[58] J. Toulouse, G. Coddens, and R. Pattnaik, Physica A **201**, 305 (1993).
[59] Y. Yang and Keith A. Nelson, Phys. Rev. Lett. **74**, 4883 (1995).
[60] S. D. Gottke, D. D. Brace, G. Hinze, and M. D. Fayer (unpublished).
[61] A. Latz provided software and assistance with the calculations.
[62] N. V. Surovtsev, J. A. H. Wiedersich, V. N. Novikov, E. Rössler, and A. P. Sokolov, Phys. Rev. B **58**, 14888 (1998).
[63] J. Gapisnki, W. Steffen, A. Patkowski, A. P. Sokolov, A. Kisliuk, U. Buchenau, M. Russina, F. Mezei, and H. Schober, J. Chem. Phys. **110**, 2312 (1999).
[64] H. C. Barshilia, G. Li, G. Q. Shen, and H. Z. Cummins, Phys. Rev. E **59**, 5625 (1999).
[65] U. Buchenau, M. Prager, N. Nücker, A. J. Dianoux, N. Ahmad, and W. A. Phillips, Phys. Rev. B **34**, 5665 (1986).
[66] A. P. Sokolov, E. Rössler, A. Kisliuk, M. Soltwisch, and D. Quitmann, Physica A **201**, 67 (1993).
[67] C. Masciovecchio, G. Ruocco, F. Sette, M. Krisch, R. Verbeni, U. Bergmann, and M. Soltwisch, Phys. Rev. Lett. **76**, 3356 (1996).
[68] M. Foret, E. Courtens, R. Vacher, and J.-B. Suck, Phys. Rev. Lett. **77**, 3831 (1996).
[69] R. C. Zeller and R. V. Pohl, Phys. Rev. B **4**, 2029 (1971).
[70] V. G. Karpov, M. I. Klinger, and F. N. Ignat'ev, Sov. Phys. JETP **57**, 439 (1983).
[71] A. P. Sokolov, J. Phys.: Condens. Matter **11**, A213 (1999).
[72] W. Schirmacher, G. Diezemann, and C. Ganter, Phys. Rev. Lett. **81**, 136 (1998).